NANO LETTERS

pubs.acs.org/NanoLett Letter

# Ultrastretchable Electrically Self-Healing Conductors Based on Silver Nanowire/Liquid Metal Microcapsule Nanocomposites

Yong Lin, Ting Fang, Chong Bai, Yuping Sun, Cheng Yang, Gaohua Hu, Haorun Guo, Weijie Qiu, Weixi Huang, Lin Wang, Zihao Tao, Yan-qing Lu,* and Desheng Kong*

Cite This: *Nano Lett.* 2023, 23, 11174−11183 Read Online

ACCESS | Metrics & More | Article Recommendations | Supporting Information

**ABSTRACT:** Stretchable conductive nanocomposites are essential for deformable electronic devices. These conductors currently face significant limitations, such as insufficient deformability, significant resistance changes upon stretching, and drifted properties during cyclic deformations. To tackle these challenges, we present an electrically self-healing and ultrastretchable conductor in the form of bilayer silver nanowire/liquid metal microcapsule nanocomposites. These nanocomposites utilize silver nanowires to establish their initial excellent conductivity. When the silver nanowire networks crack during stretching, the microcapsules are ruptured to release the encased liquid metal for recovering the electrical properties. This self-healing capability allows the nanocomposite to achieve ultrahigh stretchability for both uniaxial and biaxial strains, minor changes in resistance during stretching, and stable resistance after repetitive deformations. The conductors have been used to create skin-attachable electronic patches and stretchable light-emitting diode arrays with enhanced robustness. These developments provide a bioinspired strategy to enhance the performance and durability of conductive nanocomposites.

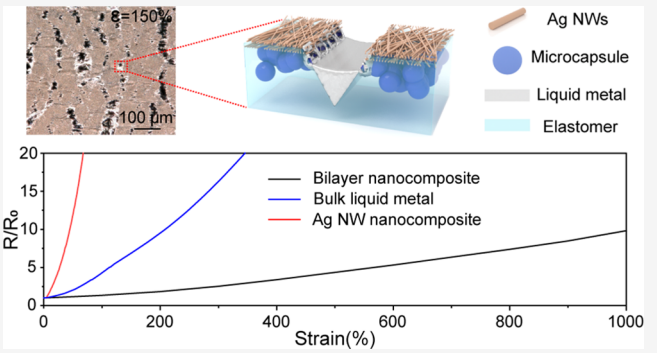


**KEYWORDS:** *self-healing, stretchable conductor, stretchable electronics, silver nanowires, liquid metal*

Stretchable electronics have emerged as a transformative technology for next-generation wearable devices.[1−3] Due to their compliant mechanical properties, these devices can establish conformal and stable interfaces with the human body, enabling promising applications in fitness monitoring,[4−6] human−machine interfaces,[7−9] and advanced prosthetics.[10,11] To create such electronics, stretchable conductors are essential as they act as the building materials for active electrodes and electrical interconnects.[12] Stretchable nanocomposites are among the most studied compliant conductors formed by dispersing various metallic nanostructures inside elastomers, including metal nanoparticles,[13] metal nanowires,[14−16] and metal nanoflakes.[17−19] These nanofillers build an electrically conductive and intrinsically stretchable percolation network in the elastomer matrix.[20] Conductive nanocomposites feature large-area fabrication and excellent electrical conductivity.[21] However, they tend to have significant resistance changes during uniaxial stretching, primarily due to the fracture of the percolation network.[22,23] Moreover, these nanocomposites may experience resistance drifts under repetitive tensile deformations due to accumulated junction damages.[24,25] In addition, conductive nanocomposites also tend to degrade rapidly under biaxial tensions that are frequently encountered in practical settings.[26,27] Therefore, addressing these performance issues is essential for the stable operation of stretchable electronics during long-term applications.

Self-healing conductors are bioinspired materials that have the ability to repair themselves after experiencing degradation and failure.[28,29] This autonomous recovery mechanism can effectively prolong the lifespan of the corresponding devices and systems. As a class of commonly used materials, intrinsically self-healing conductors are created by dispersing metallic nanostructures into soft polymers with abundant reversible bonds.[30−32] Unlike that observed in regular elastomers, the broken conductive network can be fixed by following the dynamic reconstruction of the active polymer matrix. In addition to recovery from external damage, these self-healing conductors can also restore degraded electrical properties after large and repetitive deformations,[30,33] which helps them overcome the performance limitations of traditional conductive nanocomposites. However, the autonomous reparation of the self-assembled

**Received:** September 24, 2023
**Revised:** November 29, 2023
**Accepted:** November 30, 2023
**Published:** December 4, 2023

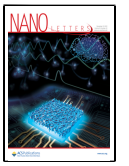

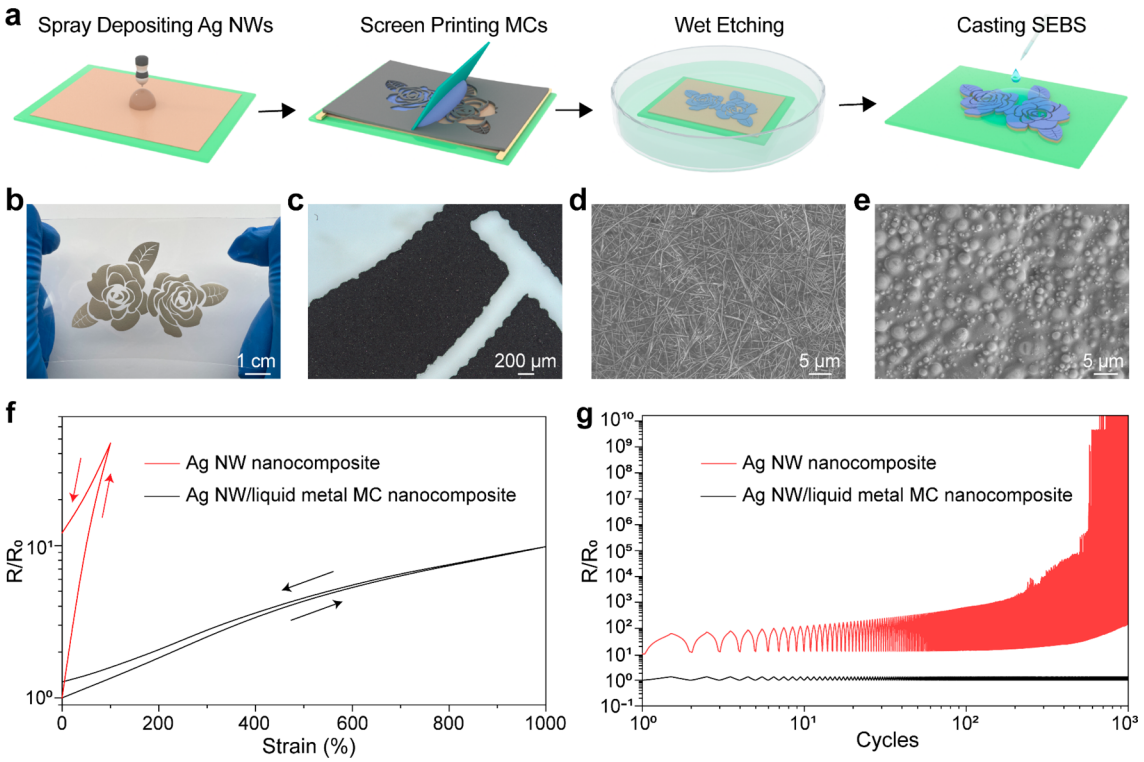


**Figure 1.** (a) Schematics illustrating the fabrication process for Ag NW/liquid metal MC nanocomposites. (b) Optical image of a stretchable flower-shaped Ag NW/liquid metal MC nanocomposite. (c) Optical microscope image showing the microstructure of the electrode. (d) Scanning electronic microscopy (SEM) image of Ag NW/SEBS nanocomposites. (e) SEM image of liquid metal MC composites. (f) Normalized resistance versus tensile strain during loading−unloading to 1000% strain. (g) Change in resistance during 1000 stretch−relaxation cycles to 100% strain.

conductive network can be time-consuming under ambient conditions due to the limited chain mobility of the polymer matrix. External activations, such as heating, light irradiations, and solvent vapor exposures,[34] are almost indispensable to speed up the healing process, which increases the overall complexity for practical applications.

Extrinsically self-healing conductors are also promising choices based on microcapsules (MCs) loaded with molten gallium-based alloys.[35,36] Liquid metals are known for their desirable properties, such as low melting points, metal-level conductivity, and liquid-like deformability.[37−41] To improve solution processability, liquid metal MCs have been top-down synthesized as microdroplets stabilized with native oxides or coordinating ligands.[42,43] It is important to note that these liquid metal microcapsules typically form insulating composites due to their surface encapsulations.[44,45] Additional mechanical activations, such as firm compression or large tensile deformations, are almost always required to rupture some microcapsules and establish electrical conductivity.[36,45] These activated conductors have demonstrated self-healing capability that arises from the release of liquid metal to connect the damaged conductive layer.[35,36] Alternatively, metallic nanoflakes have been incorporated into liquid metal composites, creating a percolation network for initial conductivity without extra activation.[46−48] Although these composites have demonstrated high conductivity and large stretchability, they are prone to significant resistance drifts during repetitive deformations. Repairing the accumulated damage in the conductive network is a major challenge in this case due to the weak coupling between embedded liquid metal MCs and metallic nanoflakes. Another attractive design for self-healing conductors involves the combination of liquid metal microcapsules with metal films.[49−51] In particular, the conformal deposition of the Cu film on liquid metal microcapsules creates conductors that can almost fully recover from structural damages caused by different levels of tensile strains.[49] However, this design tends to suffer from significant resistance changes during stretching associated with extensive cracks generated in the brittle metal films, which may lead to unstable operation of stretchable devices and systems.

In this study, we present an electrically self-healing and ultrastretchable conductor based on bilayer silver nanowire (Ag NW)/liquid metal MC nanocomposites. The patterned nanocomposite is created in a scalable printing process with a feature resolution of 100 $\mu$m. In these nanocomposites, the Ag NW network establishes the initial conductivity with a low sheet resistance of ∼0.14 Ω/sq. When subjected to large tensile deformations, MCs are effectively ruptured by the cracks in the Ag NW layer, releasing the embedded liquid metal for autonomous electrical restoration. This self-healing mechanism allows the nanocomposite to withstand a uniaxial tensile strain of 1000% and retain stable resistance during tensile fatigue tests. Notably, the resistance exhibits only minor increases with tensile strain, which is beneficial for the reliable operation of corresponding devices. Moreover, the nanocomposite can withstand biaxial tensile deformations of up to 800% area strain. The bilayer nanocomposite conductor can maintain robust properties in practical device applications, as demonstrated with a skin-attachable electronic patch and a stretchable light-emitting diode (LED) array. The developments reported here provide a generic strategy for substantial improvements in the performance and durability of stretchable conductive nanocomposites.



https://doi.org/10.1021/acs.nanolett.3c03670
Nano Lett. 2023, 23, 11174−11183

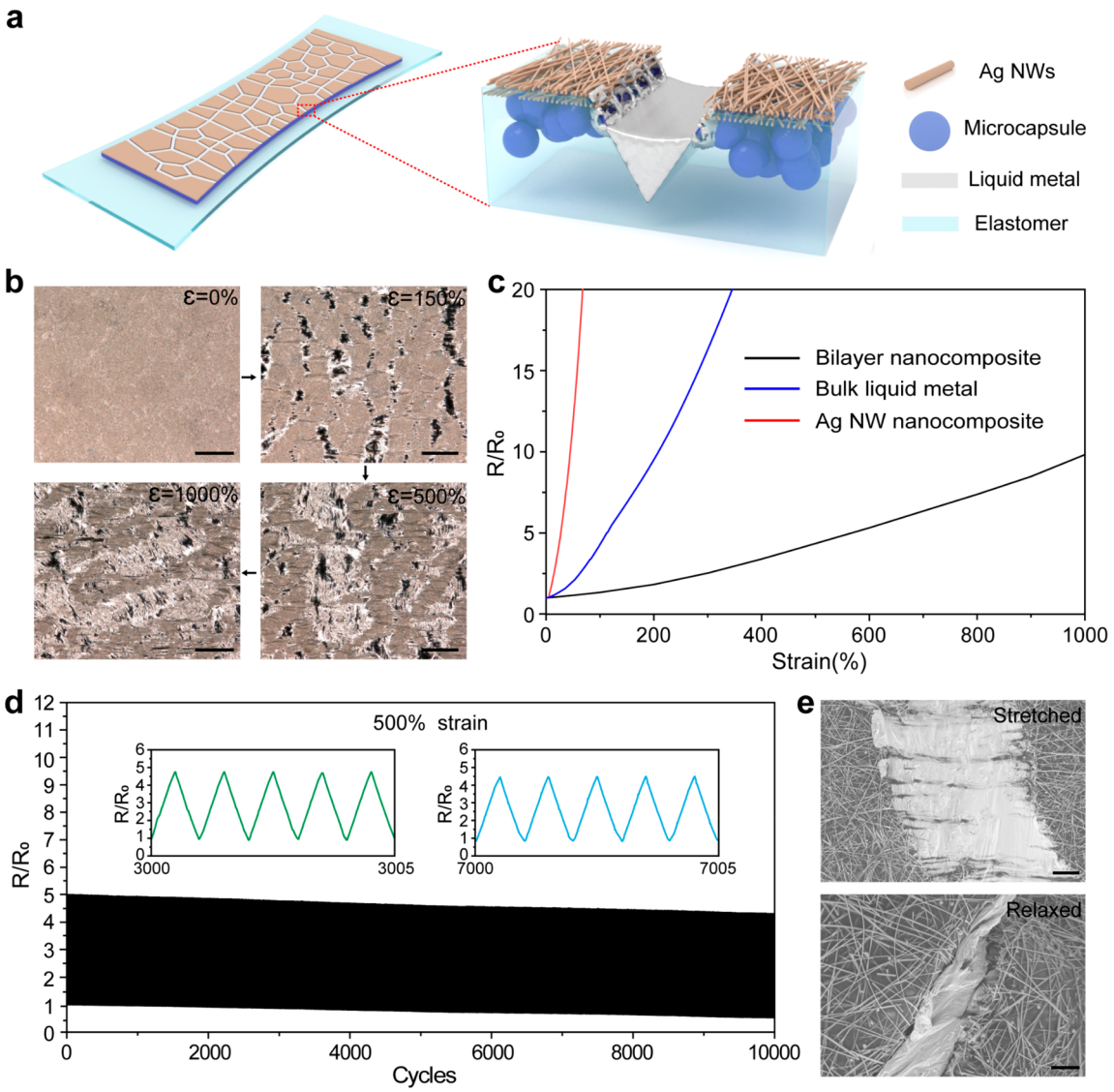


**Figure 2.** (a) Schematic illustration of the electrical healing process. (b) Optical microscopy images revealing the microstructure evolutions of the electrode in response to tensile deformations. Scale bar: 100 $\mu$m. (c) Normalized resistance versus tensile strain. (d) Change in resistance over 10000 stretch−relaxation cycles to 500% strains. Inset: Normalized resistance at cycles 3000−3005 (left) and 7000−7005 (right). (e) SEM images showing the Ag NW/liquid metal MC nanocomposites at 100% strain (top), scale bar: 5 $\mu$m, and after relaxation (bottom), scale bar: 2 $\mu$m.

Figure 1a schematically illustrates the low-cost and scalable fabrication of the conductive features. Ag NWs via polyol-reduction synthesis are spray-deposited on a nonsticky glass wafer. A top-down approach produces spherical liquid metal/fatty acid MCs with an average diameter of ~3.1 ± 1.2 $\mu$m (see Figure S1). Viscous ink is formulated by mixing these MCs with a styrene-ethylene-butylene-styrene (SEBS) elastomer solution and then screen-printed over Ag NWs. The exposed Ag NWs are easily etched away in an aqueous bath containing a mixture of ammonium hydroxide and hydrogen peroxide. During the etching process, the liquid metal MC composites act as effective etching masks to have no apparent damage (see Figure S2). SEBS solution is subsequently drop-cast to incorporate the conductive composite feature into the elastomeric substrate. Optical images were captured at each critical step of the fabrication process, as shown in Figure S3. In Figure 1b, a representative flower-shaped composite is created to demonstrate the patterning capability for arbitrary features. The optical microscopy image reveals its pixelated nature with jagged edges that is typical for screen-printed features,[52,53] as shown in Figure 1c. The patterning quality can be further improved using high mesh count screens. The overall process is pretty convenient and allows a resolution of up to 100 $\mu$m (see Figure S4). The as-prepared nanocomposite has a low sheet resistance of ~0.14 Ω/sq. Although most patterned features have consistent properties, minor confinement effects are observed for the narrowest traces at 100 $\mu$m, as depicted in Figure S5. Scanning electron microscopy (SEM) images reveal the microstructure of the top nanocomposite layer comprising Ag NWs embedded in the SEBS matrix (Figure 1d). The randomly oriented Ag NWs form a percolation network that enables excellent conductivity. In Figure 1e, the bottom layer is an electrical insulator comprising isolated liquid metal MCs. It is worth noting that this MC composite itself requires a critical strain of ~30% to activate a conductive network mechanically, as demonstrated in Figure S6. Apparently, the bilayer nanocomposite utilizes the Ag NW network to achieve the initial conductivity without any activation requirement. In Figure 1f, the resistance of the bilayer


https://doi.org/10.1021/acs.nanolett.3c03670
Nano Lett. 2023, 23, 11174−11183

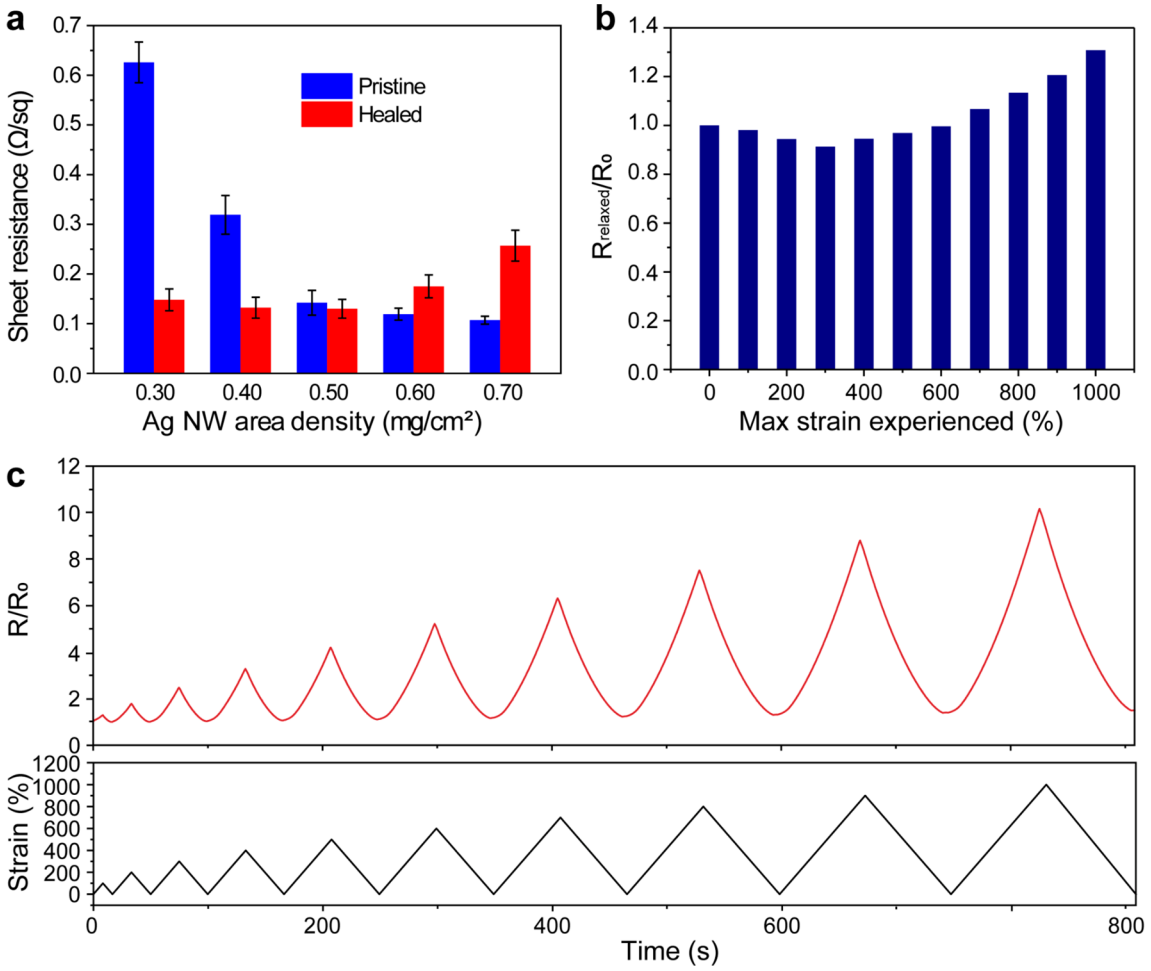


**Figure 3.** (a) Sheet resistance at the pristine and healed conditions. The Ag NW/liquid metal MC nanocomposites are subjected to 300% strain for substantial structural damage. (b) Normalized resistance of the bilayer nanocomposite at the relaxed state after experiencing different tensile strains. (c) Normalized resistance of the bilayer nanocomposite under stretch−relaxation cycles with progressively increased strains from 100% to 1000%.

nanocomposite shows limited increases under tensile deformations. Specifically, the normalized resistance is 1.3 at 100% strain, 4.6 at 500% strain, and 9.8 at 1000% strain. After the tensile strain is released, the resistance almost returns to the original value with a minor irreversible change of ∼28%. In contrast, the Ag NW nanocomposite exhibits rapidly increased resistance upon stretching, as shown in Figure 1f. The normalized resistance is 12.1 at 50% strain and 46.8 at 100% strain (Figure 1f). The resistance exhibits an irreversible increase to 12.0 times after the release of the strain (Figure 1f). Such a memory effect of strain history is commonly encountered in conductive nanocomposites through structural reconfiguration.[54,55] In the fatigue test to 100% tensile strain, the resistance of the Ag NW nanocomposite shows gradual increases in the initial 200 cycles and abrupt fluctuations in subsequent cycles (see Figure 1g). The degraded electrical properties are associated with the fracture of Ag NW networks (Figure S7).[23] However, the Ag NW/liquid metal MC nanocomposite demonstrates extremely stable resistance during 1000 stretching cycles to 100% strain (Figure 1g). Such exceptional durability has been rarely observed in conductive nanocomposites.

As schematically illustrated in Figure 2a, the conductor has a bilayer design of Ag NW networks and liquid metal MCs. The cracks in the Ag NW layer rupture the underlying MCs along their propagation paths, releasing liquid metal to recover the lost conducting pathways. According to optical microscopy images in Figure 2b, stretched nanocomposites have continuously expanded cracks of Ag NW networks that are spontaneously filled with liquid metal films. The initially released liquid metal has smooth surfaces and mirrorlike shining appearances (see Figure S8). In response to large uniaxial strains, the liquid metal film contracts transversely and creates textured surfaces with diffusive reflections, as shown in Figure S8.[56] In terms of electrical properties, regular silver nanowire nanocomposites have substantial resistance change when stretched as a result of the disconnections and cracks in the conductive network (see Figure 2c and Figure S9).[23,57−59] The bulk liquid metal confined in elastomer has the ultimate stretchability within the fracture strain.[60] Liquid metal traces have been created through direct writing, as shown in Figure S10.[61] With its constant conductivity, the bulk liquid metal still experiences significantly increased resistance upon stretching, due to a geometric effect with the combined longitude extensions and cross-sectional contractions.[62,63] The normalized resistance can be predicted using the theoretical equation $R/R_0 = (1 + \epsilon)$,[2] where $\epsilon$ is the uniaxial strain, as shown in Figure 2c and Figure S10c. In contrast, the bilayer nanocomposite allows fractured Ag NW networks to reconnect with soft liquid metal joints, which largely suppresses the resistance change along with the strain. This selective reparation of critical structural damages is illustrated in


https://doi.org/10.1021/acs.nanolett.3c03670
Nano Lett. 2023, 23, 11174−11183

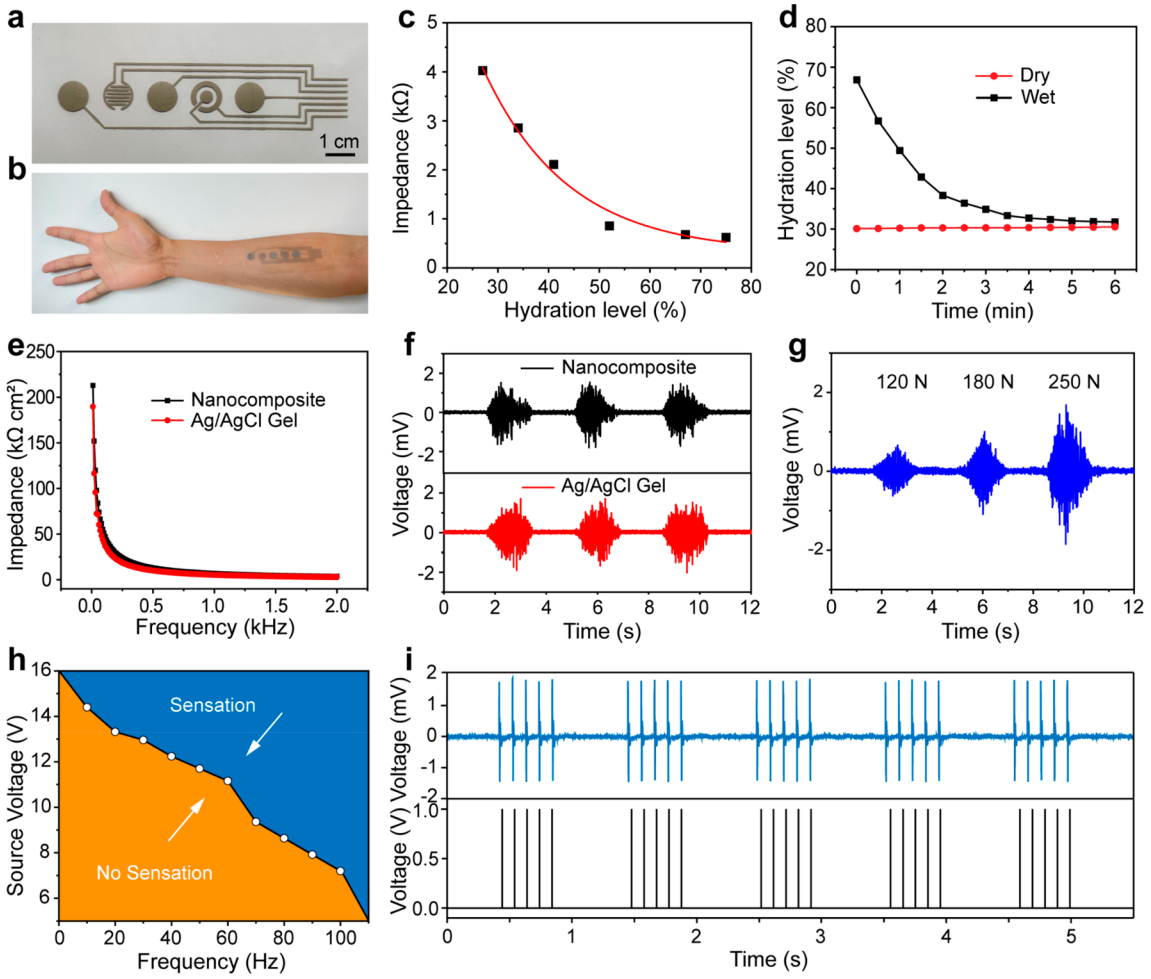


**Figure 4.** Implementing Ag NW/liquid metal MC nanocomposites in an integrated epidermal electronic patch. (a) Optical image showing a multifunctional electronic patch comprising a biopotential sensor, an electrical stimulator, and a hydration sensor. (b) Stretchable electronic patch conformally attached to the forearm. (c) Skin impedance versus skin hydration level acquired by the hydration sensor. (d) Measured skin hydration as a function of time under both dry and wet skin conditions. (e) Skin−electrode contact impedance versus the frequency for nanocomposite and commercial Ag/AgCl gel electrodes. (f) EMG waveforms of hand opening and closing gestures with 250 N grasp forces. (g) EMG waveforms acquired with nanocomposite electrodes for different grasp forces. (h) Threshold voltage for perception versus the stimulation frequency. (i) Recorded EMG waveforms (top) from the biopotential sensor during monophasic voltage pulse stimulations (bottom).

Figure 2c. The strain insensitive resistance is crucial for the reliable operation of stretchable devices and systems.[64] In addition, the conductive nanocomposite is further examined through tensile fatigue tests (Figure 2d and Figure S11). Figure 2d reveals the resistance change during 10000 stretch−relaxation cycles to 500% strain. The normalized resistances at the relaxed state are 0.98, 0.88, and 0.64 after 1000, 5000, and 10000 cycles, respectively. After 10000 cycles, the nanocomposite has a change in normalized resistance of ∼3.9 during stretching to 500% strain and is similar to the pristine sample. The fairly stable properties of the nanocomposites demonstrate exceptional durability to withstand repetitive deformations. In practice, the liquid metal joints between cracked Ag NWs are typically established under stretched states (see Figure 2e). Due to their inherent deformability, the electrical connection through these liquid metal joints is still preserved even after releasing the strain (see Figure 2e). Notice that the released liquid metal has been passivated with native oxides to avoid any apparent spread (Figure S12 in the Supporting Information).

The sheet resistance of the bilayer nanocomposite depends on the area mass density of the Ag NWs, as depicted in Figure 3a. Specifically, the sheet resistance is 0.63 ± 0.04 Ω/sq at 0.30 mg/cm$^2$, 0.14 ± 0.03 Ω/sq at 0.50 mg/cm$^2$, and 0.11 ± 0.01 Ω/sq at 0.70 mg/cm$^2$. The nanocomposites were stretched to 300% strain to induce severe structural damage. In Figure 3a, the recovered nanocomposite has reduced resistance for low Ag NW area density and increased resistance for high area density. To ensure consistent electrical properties, an intermediate density of 0.50 mg/cm$^2$ is the optimal composition and is used for subsequent experiments. The healing capability of the nanocomposite is also linked with the level of tensile deformations. Figure 3b shows the normalized resistance of the nanocomposite in the relaxed state after experiencing large tensile deformations. The relaxed conductor has reduced resistance values in response to low tensile deformations, suggesting the release of excessive liquid metals. If the tensile strain exceeds 400%, the healed resistance switches to a rising trend, likely due to the irreversible elongation of the elastomer substrate.[49] Notably, the nanocomposite retains stable resistance with less than 40% changes within 1000% strain. The conductive nanocomposite conductor is further evaluated by stretching cycles with the peak strain progressively increasing from 100% to 1000% (Figure 3c). The


https://doi.org/10.1021/acs.nanolett.3c03670
Nano Lett. 2023, 23, 11174−11183

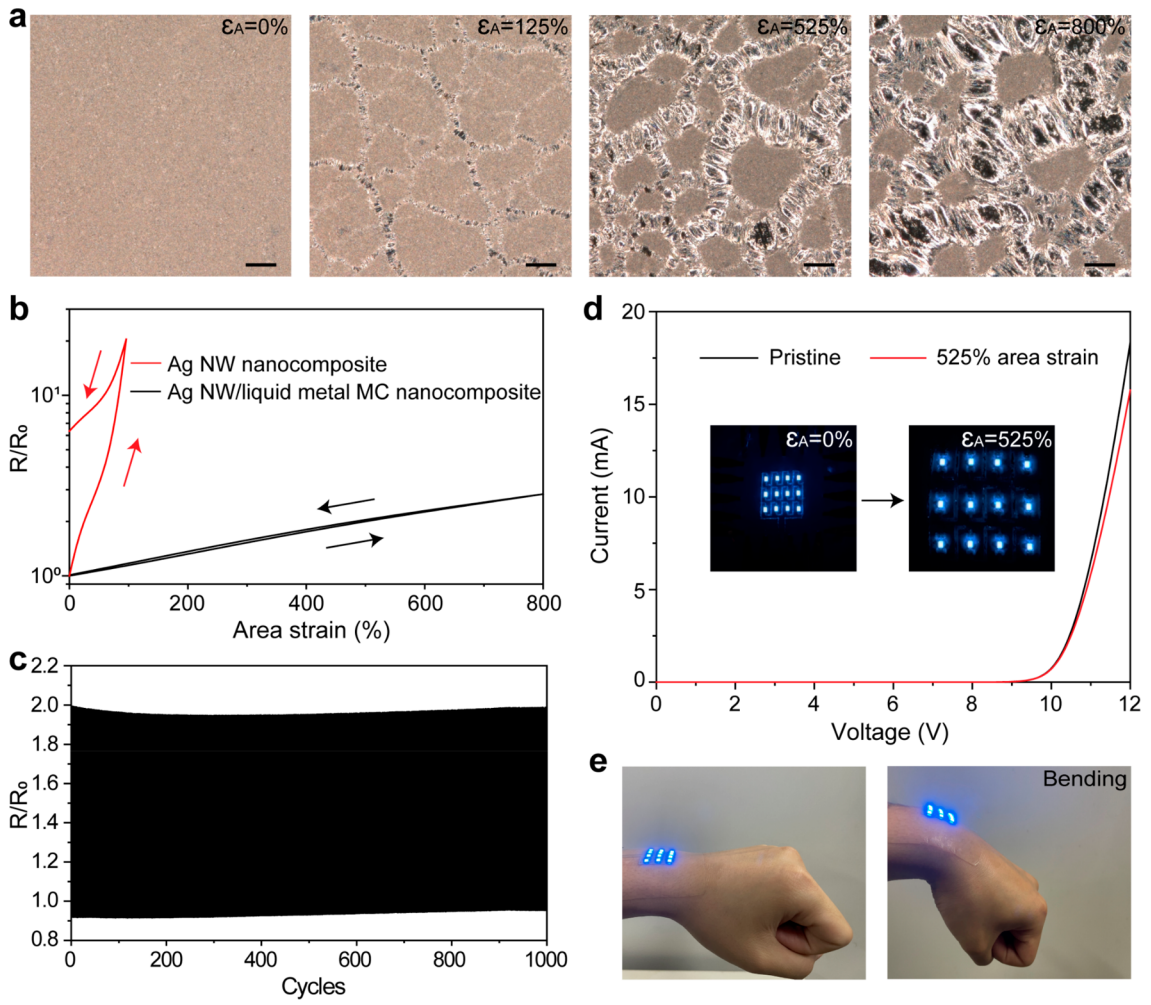


**Figure 5.** (a) Optical microscopy images revealing the microstructure evolution of Ag NW/liquid metal MC nanocomposites under biaxial tensile deformations. Scale bar: 50 $\mu$m. (b) Normalized resistance during loading−unloading to area strains for Ag NW and Ag NW/liquid metal MC nanocomposites. (c) Changes in resistance of Ag NW/liquid metal MC nanocomposites during 1000 stretch/release cycles to 525% area strains. (d) Current−voltage characteristic curves of an LED matrix at 0% and 525% area strains. Inset: Optical images of a luminous LED matrix at 0% (left) and 525% (right) area strains. (e) Optical images showing an LED matrix conformally attached to the human wrist.

normalized resistance steadily increases upon stretching and almost fully recovers after relaxation. The electrical healing capability allows the conductive nanocomposite to withstand large and unexpected deformations in practical applications.

The liquid metal MCs also play a crucial role in bilayer nanocomposites. The thickness and area densities of liquid metal MCs are controlled by the screen mesh counts. Specifically, the area densities are 17.6, 14.6, and 8.8 mg/cm$^2$ for 200, 300, and 400 meshes, respectively. The electrical properties of the corresponding bilayer nanocomposites are summarized in Figure S13. It is essential to have a high loading of liquid metal MCs for reliable self-healing properties. For nanocomposites with 14.6 and 17.6 mg/cm$^2$ MCs, the resistance shows limited changes upon stretching and negligible drifts during repetitive strain cycles. In contrast, the nanocomposite containing liquid metal MCs of 8.8 mg/cm$^2$ experiences large and irreversible changes in resistance during tensile deformations, indicating insufficient liquid metal release to fix the damaged conducting pathways. In practice, the liquid metal MC loading of 14.6 mg/cm$^2$ using 300 mesh screens is adopted for most experiments.

In the context of wearable applications, washability is a desired property of compliant conductors for hygiene purposes. The Ag NW/liquid metal MC nanocomposite is evaluated by monitoring changes in electrical properties after simulated washing cycles in the lab environment,[65,66] as shown in Figure S14. The noticeable drop in resistance upon washing is likely associated with the reduced Ag NW junction resistance by partially removing the PVP surfactant.[66] The resistance stabilizes after three laundry cycles. The observed excellent washability of the nanocomposite conductors is due to their structural stability, which is achieved by embedding them inside the elastomer substrate. In addition, the adhesion and cohesion of the nanocomposite conductor are accessed through the Scotch tape test. The conductive features retain intact structures after the tape peeling, as confirmed by visual observations and SEM characterizations (Figure S15). The resistance showed no apparent degradation upon repetitive tape peeling for up to 100 cycles. The results confirm the mechanical durability of the nanocomposites to withstand harsh operational conditions.

The bilayer nanocomposite with high conductivity and excellent mechanical deformability represents an attractive candidate material for building stretchable and wearable devices. A multifunctional electronic patch is composed of a hydration sensor, biopotential sensing electrodes, and an electrical stimulator, as shown in Figure 4a. Optical images of the critical


https://doi.org/10.1021/acs.nanolett.3c03670
Nano Lett. 2023, 23, 11174−11183

fabrication steps are displayed in Figure S16. In Figure 4b, a representative electronic patch is soft and stretchy for conformal attachment to the curvilinear surface of the human body. In Figure 4c, the hydration sensor measures the skin impedance with the interdigitated electrodes, providing a valuable indicator for skin quality and health state.[67,68] The lowered skin impedance by increasing the hydration level is associated with enhanced ionic conductivity (Figure S17 in the Supporting Information). In addition, the skin hydration level is relatively stable under indoor conditions, as shown in Figure 4d. The skin hydration rapidly increases upon application of a commercial toner and then naturally decays to reach a steady value in ∼6 min. In addition, the conductive nanocomposite has skin contact impedance similar to commercial Ag/AgCl gel electrodes, demonstrating their suitability for electrophysiological recording and simulation (see Figure 4e). The electrodes are mounted on the right flexor carpi radialis to acquire electromyogram (EMG) signals. Figure 4f reveals recorded EMG waveforms of hand open and close gestures with a ∼250 N grasp force. Specifically, the signal-to-noise ratio (SNR) is 22.3 dB for as-prepared electrodes and 22.8 dB for the commercial Ag/AgCl gel electrodes. In Figure 4g, the biopotential sensor allows the continuous measurement of EMG signals in response to different grasp forces, providing valuable information for the clinical diagnosis of muscle dysfunctions. In addition, the electrical stimulator exploits voltage pulses to induce subconscious neuromuscular responses for pain relief and physical rehabilitation.[69,70] Figure 4h reveals the electroactive perception threshold as a function of the simulation frequency. The threshold voltage is inversely related to the stimulation frequency because of the reduced contact impedance.[71] In addition to independent operations, the multifunctional patch allows simultaneous deployment of electrical stimulations and biopotential recording, as illustrated in Figure 4i. The recorded electrogram exhibits a direct correlation with stimulation pulses, providing the basis for facile monitoring of subconscious therapeutic protocols. Despite liquid metal release for electrical reparations, the lack of evident residues on the skin from the nanocomposite suggests the effective passivation of liquid metal joints with native oxides (see Figure S18a and b in the Supporting Information). The electrical healing capability of the Ag NW/liquid metal MC nanocomposite plays a vital role in the long-term stable operation of the electronic patch (see Figure S18c).

In addition to uniaxial strains, the bilayer nanocomposite is also evaluated through biaxial tensile deformations. The randomly generated cracks are filled with liquid metal without noticeable leakage, as shown in Figure 5a. The resistance increases steadily with the area strain (Figure 5b). Specifically, the normalized resistance is 1.2 at 125% area strain, 1.5 at 300% area strain, 2.0 at 525% area strain, and 2.8 at 800% area strain. After releasing the area strain, the resistance almost recovers its original value, with a slight change of approximately 2%. On the other hand, regular Ag NW nanocomposites perform poorly under area strains. The normalized resistance rapidly increases to 20.4 at 96% area strain because cracks in the Ag NW network form and expand along multiple directions (Figure 5b). An irreversible resistance increase of 6.3-fold is observed after releasing 96% area strain (see Figure 5b). The nanocomposite is also evaluated through tensile fatigue tests with different area strains (Figure 5c and Figure S19). The resistance is extremely stable during large and repetitive stretching to a 525% strain (Figure 5c). The exceptional durability is attributed to the inherent deformability of soft liquid metal joints for electrical healing capability (see Figure S20). The excellent conductivity and deformability of Ag NW/liquid metal MC nanocomposites are well-suited for constructing soft circuit systems. A representative LED matrix circuit is assembled. Briefly, the nanocomposite pattern comprising contact pads and electrical interconnects is created on a SEBS substrate. LED chips are gently mounted on the contact pads (Figure S21). Figure 5d reveals the current−voltage characteristic curves of the circuit system at 0% and 525% area strains. The limited current reduction upon stretching is ascribed to the slightly increased ohmic loss of the nanocomposite circuit. As illustrated in Figure 5d, the as-prepared circuit system provides reliable light emissions in both relaxed and highly stretched states. In Movie S1, the repetitive deformation of the LED matrix retains the stable luminous pattern under large repetitive tensile deformations, illustrating the exceptional mechanical durability of the circuit system. In Figure 5e, the LED matrix is conformally mounted on the wrist as an epidermal light source, demonstrating conformal skin attachment and reliable light emissions during joint movements. The skin-like circuit system exhibits sufficient mechanical deformability and resilience for intimate integration with the human body.

In summary, an electrically self-healing and ultrastretchable conductor is constructed in a bilayer architecture comprising Ag NW networks and the underlying liquid metal MCs. Arbitrary nanocomposite features are conveniently created in a scalable process with a decent resolution of 100 $\mu$m. Due to the percolation network of Ag NWs, the as-prepared bilayer nanocomposite has a low sheet resistance of ∼0.14 Ω/sq. The electrical self-healing capability of the nanocomposites is attributed to the release of the encased liquid metal to bridge cracks in Ag NW networks. The conductor exhibits ultrahigh stretchability to 1000% uniaxial strain, minor resistance changes with tensile strain, and excellent electromechanical durability. Notably, the conductor can easily accommodate uniaxial and biaxial tensile deformation. Their practical implementations are demonstrated by fabricating highly deformable devices with enhanced durability, including a skin-attachable electronic patch and a stretchable LED array. Combining metallic nanostructures and liquid metal MCs may open an attractive avenue to create stretchable conductive nanocomposites with exceptional performance.

## ■ ASSOCIATED CONTENT

### Supporting Information

The Supporting Information is available free of charge at https://pubs.acs.org/doi/10.1021/acs.nanolett.3c03670.

Experimental section, size distribution of liquid metal MCs, SEM image of the liquid metal MC composite before and after treatment in the etching bath, optical images illustrating the fabrication process flow, characterization of the patterning resolution, electrical properties of the bilayer nanocomposite at different line widths, resistance versus tensile strain for liquid metal MC composites, SEM images showing stretched bilayer nanocomposites, characterizations of the printed bulk liquid metal, optical microscopy image showing Ag NW nanocomposite after the uniaxial tensile fatigue test, uniaxial tensile fatigue tests on bilayer nanocomposites, structural characterizations of the bilayer nanocomposite after the uniaxial fatigue test, the influence of the liquid



https://doi.org/10.1021/acs.nanolett.3c03670
Nano Lett. 2023, 23, 11174−11183

metal MC loading on the bilayer nanocomposite, washability test, Scotch tape test, optical images showing the fabrication of the multifunctional electronic patch, impedance of the hydration sensor at different skin hydration levels, characterization of the electronic patch integrated with the human body, resistance changes of the bilayer nanocomposite during biaxial tensile fatigue tests, optical microscopy image of the bilayer nanocomposite after biaxial tensile fatigue test, and optical images showing the fabrication of the LED matrix circuit (PDF)

Dynamic deformation process of an LED matrix circuit to 525% area strain (MP4)

## AUTHOR INFORMATION


### Corresponding Authors

**Yan-qing Lu** − *College of Engineering and Applied Sciences, National Laboratory of Solid State Microstructure, and Collaborative Innovation Center of Advanced Microstructures, Nanjing University, Nanjing 210093, China; Key Laboratory of Intelligent Optical Sensing and Manipulation, Nanjing University, Nanjing 210093, China;* orcid.org/0000-0001-6151-8557; Email: yqlu@nju.edu.cn

**Desheng Kong** − *College of Engineering and Applied Sciences, National Laboratory of Solid State Microstructure, and Collaborative Innovation Center of Advanced Microstructures, Nanjing University, Nanjing 210093, China; State Key Laboratory of Analytical Chemistry for Life Science, and Jiangsu Key Laboratory of Artificial Functional Materials, Nanjing University, Nanjing 210023, China;* orcid.org/0000-0002-7339-7593; Email: dskong@nju.edu.cn

### Authors

**Yong Lin** − *College of Engineering and Applied Sciences, National Laboratory of Solid State Microstructure, and Collaborative Innovation Center of Advanced Microstructures, Nanjing University, Nanjing 210093, China; State Key Laboratory of Analytical Chemistry for Life Science, and Jiangsu Key Laboratory of Artificial Functional Materials, Nanjing University, Nanjing 210023, China*

**Ting Fang** − *College of Engineering and Applied Sciences, National Laboratory of Solid State Microstructure, and Collaborative Innovation Center of Advanced Microstructures, Nanjing University, Nanjing 210093, China; State Key Laboratory of Analytical Chemistry for Life Science, and Jiangsu Key Laboratory of Artificial Functional Materials, Nanjing University, Nanjing 210023, China*

**Chong Bai** − *College of Engineering and Applied Sciences, National Laboratory of Solid State Microstructure, and Collaborative Innovation Center of Advanced Microstructures, Nanjing University, Nanjing 210093, China; State Key Laboratory of Analytical Chemistry for Life Science, and Jiangsu Key Laboratory of Artificial Functional Materials, Nanjing University, Nanjing 210023, China;* orcid.org/0000-0001-9559-7732

**Yuping Sun** − *College of Engineering and Applied Sciences, National Laboratory of Solid State Microstructure, and Collaborative Innovation Center of Advanced Microstructures, Nanjing University, Nanjing 210093, China; State Key Laboratory of Analytical Chemistry for Life Science, and Jiangsu Key Laboratory of Artificial Functional Materials, Nanjing University, Nanjing 210023, China*

**Cheng Yang** − *College of Engineering and Applied Sciences, National Laboratory of Solid State Microstructure, and Collaborative Innovation Center of Advanced Microstructures, Nanjing University, Nanjing 210093, China; State Key Laboratory of Analytical Chemistry for Life Science, and Jiangsu Key Laboratory of Artificial Functional Materials, Nanjing University, Nanjing 210023, China*

**Gaohua Hu** − *College of Engineering and Applied Sciences, National Laboratory of Solid State Microstructure, and Collaborative Innovation Center of Advanced Microstructures, Nanjing University, Nanjing 210093, China; State Key Laboratory of Analytical Chemistry for Life Science, and Jiangsu Key Laboratory of Artificial Functional Materials, Nanjing University, Nanjing 210023, China*

**Haorun Guo** − *College of Chemical Engineering and Technology, Engineering Research Center of Seawater Utilization Technology of Ministry of Education, State Key Laboratory of Reliability and Intelligence of Electrical Equipment, Hebei University of Technology, Tianjin 300130, China*

**Weijie Qiu** − *College of Engineering and Applied Sciences, National Laboratory of Solid State Microstructure, and Collaborative Innovation Center of Advanced Microstructures, Nanjing University, Nanjing 210093, China; State Key Laboratory of Analytical Chemistry for Life Science, and Jiangsu Key Laboratory of Artificial Functional Materials, Nanjing University, Nanjing 210023, China*

**Weixi Huang** − *College of Engineering and Applied Sciences, National Laboratory of Solid State Microstructure, and Collaborative Innovation Center of Advanced Microstructures, Nanjing University, Nanjing 210093, China; State Key Laboratory of Analytical Chemistry for Life Science, and Jiangsu Key Laboratory of Artificial Functional Materials, Nanjing University, Nanjing 210023, China*

**Lin Wang** − *College of Engineering and Applied Sciences, National Laboratory of Solid State Microstructure, and Collaborative Innovation Center of Advanced Microstructures, Nanjing University, Nanjing 210093, China; State Key Laboratory of Analytical Chemistry for Life Science, and Jiangsu Key Laboratory of Artificial Functional Materials, Nanjing University, Nanjing 210023, China*

**Zihao Tao** − *Kuang Yaming Honors School, Nanjing University, Nanjing 210023, China*

Complete contact information is available at: https://pubs.acs.org/10.1021/acs.nanolett.3c03670


### Author Contributions

The manuscript was written through contributions of all authors. All authors have given approval to the final version of the manuscript.

### Notes

The authors declare no competing financial interest.

## ACKNOWLEDGMENTS

We acknowledge the support from the National Key Research and Development Program of China (Grant No. 2022YFA1405000), the Natural Science Foundation of Jiangsu Province, Major Project (Grant No. BK20212004), and the National Natural Science Foundation of China (Grant No. 62374083).

## REFERENCES


(1) Rogers, J. A.; Someya, T.; Huang, Y. Materials and mechanics for stretchable electronics. *Science* **2010**, *327* (5973), 1603−1607.

(2) Wang, S.; Oh, J. Y.; Xu, J.; Tran, H.; Bao, Z. Skin-Inspired Electronics: An Emerging Paradigm. *Acc. Chem. Res.* **2018**, *51* (5), 1033−1045.

(3) Ma, Z.; Kong, D.; Pan, L.; Bao, Z. Skin-inspired Electronics: Emerging Semiconductor Devices and Systems. *J. Semicond.* **2020**, *41* (4), 041601.

(4) Chung, H. U.; Kim, B. H.; Lee, J. Y.; Lee, J.; Xie, Z.; Ibler, E. M.; Lee, K.; Banks, A.; Jeong, J. Y.; Kim, J.; Ogle, C.; Grande, D.; Yu, Y.; Jang, H.; Assem, P.; Ryu, D.; Kwak, J. W.; Namkoong, M.; Park, J. B.; Lee, Y.; Kim, D. H.; Ryu, A.; Jeong, J.; You, K.; Ji, B.; Liu, Z.; Huo, Q.; Feng, X.; Deng, Y.; Xu, Y.; Jang, K.-I.; Kim, J.; Zhang, Y.; Ghaffari, R.; Rand, C. M.; Schau, M.; Hamvas, A.; Weese-Mayer, D. E.; Huang, Y.; Lee, S. M.; Lee, C. H.; Shanbhag, N. R.; Paller, A. S.; Xu, S.; Rogers, J. A. Binodal, wireless epidermal electronic systems with in-sensor analytics for neonatal intensive care. *Science* **2019**, *363* (6430), No. eaau0780.

(5) Lee, G.-H.; Woo, H.; Yoon, C.; Yang, C.; Bae, J.-Y.; Kim, W.; Lee, D. H.; Kang, H.; Han, S.; Kang, S.-K.; Park, S.; Kim, H.-R.; Jeong, J.-W.; Park, S. A Personalized Electronic Tattoo for Healthcare Realized by On-the-Spot Assembly of an Intrinsically Conductive and Durable Liquid-Metal Composite. *Adv. Mater.* **2022**, *34* (32), 2204159.

(6) Wang, S.; Nie, Y.; Zhu, H.; Xu, Y.; Cao, S.; Zhang, J.; Li, Y.; Wang, J.; Ning, X.; Kong, D. Intrinsically stretchable electronics with ultrahigh deformability to monitor dynamically moving organs. *Sci. Adv.* **2022**, *8* (13), No. eabl5511.

(7) Wang, M.; Yan, Z.; Wang, T.; Cai, P.; Gao, S.; Zeng, Y.; Wan, C.; Wang, H.; Pan, L.; Yu, J.; Pan, S.; He, K.; Lu, J.; Chen, X. Gesture recognition using a bioinspired learning architecture that integrates visual data with somatosensory data from stretchable sensors. *Nat. Electron.* **2020**, *3* (9), 563−570.

(8) Zhao, H.; Zhou, Y.; Cao, S.; Wang, Y.; Zhang, J.; Feng, S.; Wang, J.; Li, D.; Kong, D. Ultrastretchable and Washable Conductive Microtextiles by Coassembly of Silver Nanowires and Elastomeric Microfibers for Epidermal Human-Machine Interfaces. *ACS Material Lett.* **2021**, *3* (7), 912−920.

(9) Kim, K. K.; Kim, M.; Pyun, K.; Kim, J.; Min, J.; Koh, S.; Root, S. E.; Kim, J.; Nguyen, B.-N. T.; Nishio, Y.; Han, S.; Choi, J.; Kim, C. Y.; Tok, J. B.-H.; Jo, S.; Ko, S. H.; Bao, Z. A Substrate-Less Nanomesh Receptor with Meta-Learning for Rapid Hand Task Recognition. *Nat. Electron.* **2022**, *6* (1), 64−75.

(10) Kim, J.; Lee, M.; Shim, H. J.; Ghaffari, R.; Cho, H. R.; Son, D.; Jung, Y. H.; Soh, M.; Choi, C.; Jung, S.; Chu, K.; Jeon, D.; Lee, S. T.; Kim, J. H.; Choi, S. H.; Hyeon, T.; Kim, D. H. Stretchable Silicon Nanoribbon Electronics for Skin Prosthesis. *Nat. Commun.* **2014**, *5* (1), 5747.

(11) Chortos, A.; Liu, J.; Bao, Z. Pursuing Prosthetic Electronic Skin. *Nat. Mater.* **2016**, *15* (9), 937−950.

(12) Matsuhisa, N.; Chen, X.; Bao, Z.; Someya, T. Materials and Structural Designs of Stretchable Conductors. *Chem. Soc. Rev.* **2019**, *48* (11), 2946−2966.

(13) Kim, Y.; Zhu, J.; Yeom, B.; Di Prima, M.; Su, X.; Kim, J.-G.; Yoo, S. J.; Uher, C.; Kotov, N. A. Stretchable nanoparticle conductors with self-organized conductive pathways. *Nature* **2013**, *500* (7460), 59−63.

(14) Xu, F.; Zhu, Y. Highly Conductive and Stretchable Silver Nanowire Conductors. *Adv. Mater.* **2012**, *24* (37), 5117−5122.

(15) Choi, S.; Han, S. I.; Jung, D.; Hwang, H. J.; Lim, C.; Bae, S.; Park, O. K.; Tschabrunn, C. M.; Lee, M.; Bae, S. Y.; Yu, J. W.; Ryu, J. H.; Lee, S.-W.; Park, K.; Kang, P. M.; Lee, W. B.; Nezafat, R.; Hyeon, T.; Kim, D.-H. Highly conductive, stretchable and biocompatible Ag-Au core-sheath nanowire composite for wearable and implantable bioelectronics. *Nat. Nanotechnol.* **2018**, *13* (11), 1048−1056.

(16) Liang, J.; Li, L.; Niu, X.; Yu, Z.; Pei, Q. Elastomeric Polymer Light-emitting Devices and Displays. *Nat. Photonics* **2013**, *7* (10), 817−824.

(17) Guo, W.; Zheng, P.; Huang, X.; Zhuo, H.; Wu, Y.; Yin, Z.; Li, Z.; Wu, H. Matrix-Independent Highly Conductive Composites for Electrodes and Interconnects in Stretchable Electronics. *ACS Appl. Mater. Interfaces* **2019**, *11* (8), 8567−8575.

(18) Ding, C.; Wang, J.; Yuan, W.; Zhou, X.; Lin, Y.; Zhu, G.; Li, J.; Zhong, T.; Su, W.; Cui, Z. Durability Study of Thermal Transfer Printed Textile Electrodes for Wearable Electronic Applications. *ACS Appl. Mater. Interfaces* **2022**, *14* (25), 29144−29155.

(19) Matsuhisa, N.; Inoue, D.; Zalar, P.; Jin, H.; Matsuba, Y.; Itoh, A.; Yokota, T.; Hashizume, D.; Someya, T. Printable elastic conductors by in situ formation of silver nanoparticles from silver flakes. *Nat. Mater.* **2017**, *16* (8), 834−840.

(20) Yao, S.; Zhu, Y. Nanomaterial-Enabled Stretchable Conductors: Strategies, Materials and Devices. *Adv. Mater.* **2015**, *27* (9), 1480−1511.

(21) Choi, S.; Han, S. I.; Kim, D.; Hyeon, T.; Kim, D. H. High performance Stretchable Conductive Nanocomposites: Materials, Processes, and Device applications. *Chem. Soc. Rev.* **2019**, *48* (6), 1566−1595.

(22) Matsuhisa, N.; Kaltenbrunner, M.; Yokota, T.; Jinno, H.; Kuribara, K.; Sekitani, T.; Someya, T. Printable Elastic Conductors with a High Conductivity for Electronic Textile Applications. *Nat. Commun.* **2015**, *6* (1), 7461.

(23) Jung, D.; Lim, C.; Park, C.; Kim, Y.; Kim, M.; Lee, S.; Lee, H.; Kim, J. H.; Hyeon, T.; Kim, D. Adaptive Self-Organization of Nanomaterials Enables Strain-Insensitive Resistance of Stretchable Metallic Nanocomposites. *Adv. Mater.* **2022**, *34* (23), 2200980.

(24) Jin, H.; Nayeem, M. O. G.; Lee, S.; Matsuhisa, N.; Inoue, D.; Yokota, T.; Hashizume, D.; Someya, T. Highly Durable Nanofiber-Reinforced Elastic Conductors for Skin-Tight Electronic Textiles. *ACS Nano* **2019**, *13* (7), 7905−7912.

(25) Lin, Y.; Li, Q.; Ding, C.; Wang, J.; Yuan, W.; Liu, Z.; Su, W.; Cui, Z. High-Resolution and Large-size Stretchable Electrodes Based on Patterned Silver Nanowires Composites. *Nano Res.* **2022**, *15* (5), 4590−4598.

(26) Kim, B. S.; Pyo, J. B.; Son, J. G.; Zi, G.; Lee, S. S.; Park, J. H.; Lee, J. Biaxial Stretchability and Transparency of Ag Nanowire 2D Mass-Spring Networks Prepared by Floating Compression. *ACS Appl. Mater. Interfaces* **2017**, *9* (12), 10865−10873.

(27) Wu, C.; Jiu, J.; Araki, T.; Koga, H.; Sekitani, T.; Wang, H.; Suganuma, K. Biaxially Stretchable Silver Nanowire Conductive Film Embedded in a Taro Leaf-templated PDMS Surface. *Nanotechnology* **2017**, *28* (1), 01LT01.

(28) Kang, J.; Tok, J. B.-H.; Bao, Z. Self-Healing Soft Electronics. *Nat. Electron.* **2019**, *2* (4), 144−150.

(29) Luo, C. S.; Wan, P.; Yang, H.; Shah, S. A. A.; Chen, X. Healable Transparent Electronic Devices. *Adv. Funct. Mater.* **2017**, *27* (23), 1606339.

(30) Son, D.; Kang, J.; Vardoulis, O.; Kim, Y.; Matsuhisa, N.; Oh, J. Y.; To, J. W.; Mun, J.; Katsumata, T.; Liu, Y.; McGuire, A. F.; Krason, M.; Molina-Lopez, F.; Ham, J.; Kraft, U.; Lee, Y.; Yun, Y.; Tok, J. B.-H.; Bao, Z. An Integrated Self-Healable Electronic Skin System Fabricated via Dynamic Reconstruction of a Nanostructured Conducting Network. *Nat. Nanotechnol.* **2018**, *13* (11), 1057−1065.

(31) Tee, C. K.; Wang, C.; Allen, R.; Bao, Z. An electrically and mechanically self-healing composite with pressure and flexion-sensitive properties for electronic skin applications. *Nat. Nanotechnol.* **2012**, *7* (12), 825−832.

(32) Song, P.; Qin, H.; Gao, H. L.; Cong, H. P.; Yu, S. H. Self-Healing and Superstretchable Conductors from Hierarchical Nanowire Assemblies. *Nat. Commun.* **2018**, *9* (1), 2786.

(33) Kim, S. H.; Seo, H.; Kang, J.; Hong, J.; Seong, D.; Kim, H. J.; Kim, J.; Mun, J.; Youn, I.; Kim, J.; Kim, Y. C.; Seok, H. K.; Lee, C.; Tok, J. B.; Bao, Z.; Son, D. An Ultrastretchable and Self-Healable Nanocomposite Conductor Enabled by Autonomously Percolative Electrical Pathways. *ACS Nano* **2019**, *13* (6), 6531−6539.

(34) Benight, S. J.; Wang, C.; Tok, J. B. H.; Bao, Z. Stretchable and Self-Healing Polymers and Devices for Electronic Skin. *Prog. Polym. Sci.* **2013**, *38* (12), 1961−1977.




https://doi.org/10.1021/acs.nanolett.3c03670
*Nano Lett.* 2023, 23, 11174−11183

(35) Blaiszik, B. J.; Kramer, S. L. B.; Grady, M. E.; McIlroy, D. A.; Moore, J. S.; Sottos, N. R.; White, S. R. Autonomic Restoration of Electrical Conductivity. *Adv. Mater.* **2012**, *24* (3), 398−401.
(36) Markvicka, E. J.; Bartlett, M. D.; Huang, X.; Majidi, C. An Autonomously Electrically Self-Healing Liquid Metal-Elastomer Composite for Robust Soft-Matter Robotics and Electronics. *Nat. Mater.* **2018**, *17* (7), 618−624.
(37) Dickey, M. D. Stretchable and Soft Electronics Using Liquid Metals. *Adv. Mater.* **2017**, *29* (27), 1606425.
(38) Handschuh-Wang, S.; Stadler, F. J.; Zhou, X. Critical Review on the Physical Properties of Gallium-Based Liquid Metals and Selected Pathways for Their Alteration. *J. Phys. Chem. C* **2021**, *125* (37), 20113−20142.
(39) Kazem, N.; Hellebrekers, T.; Majidi, C. Soft Multifunctional Composites and Emulsions with Liquid Metals. *Adv. Mater.* **2017**, *29* (27), 1605985.
(40) Chen, S.; Wang, H.-Z.; Zhao, R.-Q.; Rao, W.; Liu, J. Liquid Metal Composites. *Matter* **2020**, *2* (6), 1446−1480.
(41) Zhuang, Q.; Ma, Z.; Gao, Y.; Zhang, Y.; Wang, S.; Lu, X.; Hu, H.; Cheung, C.; Huang, Q.; Zheng, Z. Liquid-Metal-Superlyophilic and Conductivity-Strain-Enhancing Scaffold for Permeable Superelastic Conductors. *Adv. Funct. Mater.* **2021**, *31* (47), 2105587.
(42) Li, Y.; Feng, S.; Cao, S.; Zhang, J.; Kong, D. Printable Liquid Metal Microparticle Ink for Ultrastretchable Electronics. *ACS Appl. Mater. Interfaces* **2020**, *12* (45), 50852−50859.
(43) Hohman, J. N.; Kim, M.; Wadsworth, G. A.; Bednar, H. R.; Jiang, J.; LeThai, M. A.; Weiss, P. S. Directing Substrate Morphology via Self Assembly: Ligand-Mediated Scission of Gallium-Indium Microspheres to the Nanoscale. *Nano Lett.* **2011**, *11* (12), 5104−5110.
(44) Boley, J. W.; White, E. L.; Kramer, R. K. Mechanically Sintered Gallium-Indium Nanoparticles. *Adv. Mater.* **2015**, *27* (14), 2355−2360.
(45) Mou, L.; Qi, J.; Tang, L.; Dong, R.; Xia, Y.; Gao, Y.; Jiang, X. Highly Stretchable and Biocompatible Liquid Metal-Elastomer Conductors for Self-Healing Electronics. *Small* **2020**, *16* (51), 2005336.
(46) Wang, J.; Cai, G.; Li, S.; Gao, D.; Xiong, J.; Lee, P. S. Printable Superelastic Conductors with Extreme Stretchability and Robust Cycling Endurance Enabled by Liquid-Metal Particles. *Adv. Mater.* **2018**, *30* (16), 1706157.
(47) Lopes, P. A.; Fernandes, D. F.; Silva, A. F.; Marques, D. G.; de Almeida, A. T.; Majidi, C.; Tavakoli, M. Bi-Phasic Ag-In-Ga-Embedded Elastomer Inks for Digitally Printed, Ultra-Stretchable, Multi-Layer Electronics. *ACS Appl. Mater. Interfaces* **2021**, *13* (12), 14552−14561.
(48) Hajalilou, A.; Silva, A. F.; Lopes, P. A.; Parvini, E.; Majidi, C.; Tavakoli, M. Biphasic Liquid Metal Composites for Sinter-Free Printed Stretchable Electronics. *Adv. Mater. Interfaces* **2022**, *9* (5), 2101913.
(49) Li, Y.; Fang, T.; Zhang, J.; Zhu, H.; Sun, Y.; Wang, S.; Lu, Y.; Kong, D. Ultrasensitive and ultrastretchable electrically self-healing conductors. *Proc. Natl. Acad. Sci. U. S. A.* **2023**, *120* (23), No. e2300953120.
(50) Chen, K.; Zhang, L.; Wu, K.; Yang, C.; Wang, R.; Xu, C.; Zhang, J.; Liu, G.; Sun, J. Highly Robust and Strain-Resilient Thin Film Conductors Featuring Brittle Materials. *Nano Lett.* **2023**, *23* (14), 6619−6628.
(51) Li, G.; Ma, X.; Xu, Z.; Shen, Y.; Yuan, M.; Huang, J.; Cole, T.; Wei, J.; Liu, S.; Han, F.; Li, H.; Bayinqiaoge; Xu, Z.; Tang, S. Y.; Liu, Z. A Crack Compensation Strategy for Highly Stretchable Conductors Based on Liquid Metal Inclusions. *iScience* **2022**, *25* (12), 105495.
(52) Zhu, H.; Wang, S.; Zhang, M.; Li, T.; Hu, G.; Kong, D. Fully solution processed liquid metal features as highly conductive and ultrastretchable conductors. *npj Flexible Electron.* **2021**, *5* (1), 25.
(53) Zhao, C. S.; Zhou, Y. L.; Gu, S. Q.; Cao, S. T.; Wang, J. C.; Zhang, M. H.; Wu, Y. Z.; Kong, D. S. Fully screen-printed, multicolor, and stretchable electroluminescent displays for epidermal electronics. *ACS Appl. Mater. Interfaces* **2020**, *12* (42), 47902−47910.
(54) Yuan, W.; Wu, X.; Gu, W.; Lin, J.; Cui, Z. Printed Stretchable Circuit on Soft Elastic Substrate for Wearable Application. *J. Semicond.* **2018**, *39* (1), 015002.
(55) Lipomi, D. J.; Vosgueritchian, M.; Tee, B. C.; Hellstrom, S. L.; Lee, J. A.; Fox, C. H.; Bao, Z. Skin-Like Pressure and Strain Sensors Based on Transparent Elastic Films of Carbon Nanotubes. *Nat. Nanotechnol.* **2011**, *6* (12), 788.
(56) Zhang, J.; Lu, Q.; Li, Y.; Li, T.; Lu, M.-H.; Chen, Y.-F.; Kong, D. An Ultrastretchable Reflective Electrode Based on a Liquid Metal Film for Deformable Optoelectronics. *ACS Mater. Lett.* **2021**, *3* (8), 1104−1111.
(57) Bae, J.-S.; Lee, Y.-S.; Li, J.; Liang, J.; Chen, D.; Pei, Q.; Lee, S.-B. The Feasibility of Healable Electronics and Mechanical Behavior of Silver Nanowire (AgNW)/Healable Polymer Composite. *Adv. Mater. Technol.* **2018**, *3* (6), 1700364.
(58) Schrenker, N. J.; Xie, Z.; Schweizer, P.; Moninger, M.; Werner, F.; Karpstein, N.; Mačković, M.; Spyropoulos, G. D.; Göbelt, M.; Christiansen, S.; Brabec, C. J.; Bitzek, E.; Spiecker, E. Microscopic Deformation Modes and Impact of Network Anisotropy on the Mechanical and Electrical Performance of Five-fold Twinned Silver Nanowire Electrodes. *ACS Nano* **2021**, *15* (1), 362−376.
(59) Huang, G. W.; Xiao, H. M.; Fu, S. Y. Wearable Electronics of Silver-Nanowire/Poly(dimethylsiloxane) Nanocomposite for Smart Clothing. *Sci. Rep.* **2015**, *5* (1), 13971.
(60) Ota, H.; Chen, K.; Lin, Y.; Kiriya, D.; Shiraki, H.; Yu, Z.; Ha, T.-J.; Javey, A. Highly Deformable Liquid-State Heterojunction Sensors. *Nat. Commun.* **2014**, *5* (1), 5032.
(61) Boley, J. W.; White, E. L.; Chiu, G. T. C.; Kramer, R. K. Direct Writing of Gallium-Indium Alloy for Stretchable Electronics. *Adv. Funct. Mater.* **2014**, *24* (23), 3501−3507.
(62) Matsuzaki, R.; Tabayashi, K. Highly Stretchable, Global, and Distributed Local Strain Sensing Line Using GaInSn Electrodes for Wearable Electronics. *Adv. Funct. Mater.* **2015**, *25* (25), 3806−3813.
(63) Hu, G.; Zhu, H.; Guo, H.; Wang, S.; Sun, Y.; Zhang, J.; Lin, Y.; Kong, D. Maskless Fabrication of Highly Conductive and Ultra-stretchable Liquid Metal Features through Selective Laser Activation. *ACS Appl. Mater. Interfaces* **2023**, *15* (23), 28675−28683.
(64) Liu, S. Z.; Shah, D. S.; Kramer-Bottiglio, R. Highly Stretchable Multilayer Electronic Circuits Using Biphasic Gallium-Indium. *Nat. Mater.* **2021**, *20* (6), 851−858.
(65) Hsu, P. C.; Liu, X.; Liu, C.; Xie, X.; Lee, H.; Welch, A. J.; Zhao, T.; Cui, Y. Personal Thermal Management by Metallic Nanowire-Coated Textile. *Nano Lett.* **2015**, *15* (1), 365−371.
(66) Lee, Y.; Bae, S.; Hwang, B.; Schroeder, M.; Lee, Y.; Baik, S. Considerably Improved Water and Oil Washability of Highly Conductive Stretchable Fibers by Chemical Functionalization with Fluorinated Silane. *J. Mater. Chem. C* **2019**, *7* (39), 12297−12305.
(67) Hon, K.-l. E.; Wong, K. Y.; Leung, T.-f.; Chow, C.-m.; Ng, P.-c. Comparison of Skin Hydration Evaluation Sites and Correlations among Skin Hydration, Transepidermal Water Loss, SCORAD Index, Nottingham Eczema Severity Score, and Quality of Life in Patients with Atopic Dermatitis. *Am. J. Clin. Dermatol.* **2008**, *9* (1), 45−50.
(68) Kleiner, S. M. Water: An Essential But Overlooked Nutrient. *J. Am. Diet. Assoc.* **1999**, *99* (2), 200−206.
(69) Hurley, M. V.; Bearne, L. M. Non-exercise physical therapies for musculoskeletal conditions. *Best Pract. Res., Clin. Rheumatol.* **2008**, *22* (3), 419−433.
(70) Sarzi-Puttini, P.; Cimmino, M. A.; Scarpa, R.; Caporali, R.; Parazzini, F.; Zaninelli, A.; Atzeni, F.; Canesi, B. Osteoarthritis: An Overview of the Disease and Its Treatment Strategies. *Semin. ArthritisRheum.* **2005**, *35* (1), 1−10.
(71) Lim, S.; Son, D.; Kim, J.; Lee, Y. B.; Song, J.-K.; Choi, S.; Lee, D. J.; Kim, J. H.; Lee, M.; Hyeon, T.; et al. Transparent and Stretchable Interactive Human Machine Interface Based on Patterned Graphene Heterostructures. *Adv. Funct. Mater.* **2015**, *25* (3), 375−383.


https://doi.org/10.1021/acs.nanolett.3c03670
*Nano Lett.* 2023, 23, 11174−11183